Mechanically Tunable Elastic Modulus of Freestanding $Ba_{1-x}Sr_xTiO_3$ Membranes via Phase-field Simulation

Kena Zhang¹, Yao Ren¹, Ye Cao^{1*}

¹Department of Materials Science and Engineering, University of Texas at Arlington, Arlington,

TX, 76019

Corresponding author: Ye Cao

*Email: <u>ye.cao@uta.edu</u>

Phone: +1 8172721858

Address: ELB 332, 501 West First St., Arlington, TX, 76019

Abstract

The freestanding ferroelectric membranes with super-elasticity shows promising applications in flexible electronic devices such as transducers, memories, etc. While there have been recent studies on the effect of mechanical bending on the domain structure evolutions and phase transitions in ferroelectric membranes, its influence on the Young's modulus of these freestanding membranes is less explored, which is crucial for the design and application of flexible electronics. Here, a phase-field model is developed to simulate the tunability of Young's modulus of freestanding Ba_{1-x}Sr_xTiO₃ membranes under mechanical bending. It is demonstrated that the bended membrane shows a uniform Young's modulus compared with unbended membrane. By increasing the bending angle, the Young's modulus tunability is enhanced, which can be attributed to the vortex-like domain structures induced by the mechanical bending. These vortex-like domains with large domain wall energy inhibit the subsequent domain switching under externally applied tensile strain and reduce the eigenstrain variation, which leads to a large Young's modulus. In addition, the formation of vortex domain structure is suppressed with increasing Sr²⁺ content in Ba_{1-x}Sr_xTiO₃ membranes at the same bending degree, resulting in a decrease in the Young's modulus tunability. Our work reveals that the tunability of Young's modulus of freestanding ferroelectric membranes can be achieved by mechanical bending, which provides a guidance for designing the flexible electronic devices.

Ferroelectric oxides with spontaneous and re-orientable electrical polarization have attracted intensive attention due to its wide applications in energy storage devices^{1,2}, sensors³, tunable phononic crystals⁴, and memory devices^{5,6}. The ferroelectric domain structure and domain switching play a dominant role in determining its functional properties. Various external stimuli, such as electrical, optical, magnetic, and mechanical excitations have been employed to dynamically tune the ferroelectric functionalities via controlling the ferroelectric domain structure⁷⁻¹⁰. Among them, the externally applied mechanical load is commonly used due to the intrinsic electromechanical properties in ferroelectrics^{11–14}. With the introduction of strain to the lattice, the ability of polarization can be changed. Consequently, signals can be controlled by the mechanical strain which provides a simple way to realize the modulation of materials properties and corresponding device functionalities. Due to the fact that ferroelectric oxides are intrinsically brittle, existing mechanical excitation mainly employs the lattice mismatch between the ferroelectric thin film and the substrate, or via a local tip force from the probe of a piezoresponse force microscope (PFM)¹⁵⁻¹⁷. However, there is a limitation on the generation of large deformation due to the substrate constraint or the limited area of a local tip force.

Recently, several experimental works demonstrated that the super-elasticity in ferroelectric oxides can be achieved by fabricating freestanding ferroelectric membranes. These membranes show extremely large bending deformations without any cracks^{18,19}. The freestanding crystalline oxide membranes develop an additional degree of freedom of large strain-triggered correlated phenomena. Dong *et al.*¹⁸ investigated the ferroelectric domain evolution and the piezoelectric response of the flexible freestanding BaTiO₃ membranes.

Peng *et al.*²⁰ studied the domain patterns and phase transition of BiFeO₃ membranes and constructed a phase diagram as a function of bending angle. Ko *et al.*²¹ reported a high dielectric tunability from -77.8% to 34% in Ba_{0.5}Sr_{0.5}TiO₃ membranes under mechanical bending. Although several researchers have investigated the ferroelectric domain evolution^{11,22}, dielectric constant tunability²¹, and phase transition²³ in ferroelectric membranes via mechanical bending, the response of the mechanical properties, such as the Young's modulus to mechanical bending is less explored and not fully understood. The Young's modulus of ferroelectric materials is the key factor in their applications in the tunable resonators, transducers, and phononic crystals, etc. Therefore, it is crucial to understand how the Young's modulus is dependent on the mechanical bending in ferroelectric membranes.

Among various inorganic ferroelectric oxides, strain-sensitive $Ba_{1-x}Sr_xTiO_3$ perovskite is one of the most potential candidates for flexible electronic device application due to its intensive strain sensitivity^{12,13,21}. In addition, due to the difference of ionic radius between Sr^{2+} and Ba^{2+} , a ferroelectric-paraelectric transition occurs at the Sr^{2+} composition ($x \sim 0.3$) at room temperature, which affects the magnitude of local polarization and domain structure²⁴. Thus, in this work, $Ba_{1-x}Sr_xTiO_3$ is selected as the model system to investigate the mechanically tunable Young's modulus using phase-field simulation. The dynamical tunability of the Young's modulus of $Ba_{1-x}Sr_xTiO_3$ membranes via mechanical bending under different bending angles is systematically studied. In addition, the effect of Sr^{2+} content in the $Ba_{1-x}Sr_xTiO_3$ system on the tunability of Young's modulus is further investigated. Finally, the fundamental mechanism of Young's modulus tunability due to the contributions of domain structure evolution and phase transition is explored.

A phase-field model is developed to simulate the ferroelectric properties of the Ba_{1-x}Sr_xTiO₃ freestanding membranes. The temporal evolution of polarization $P_i = (P_1, P_2, P_3)$ is solved by the time-dependent Ginzburg-Landau (TDGL) equation,

$$\frac{\partial P_i(r,t)}{\partial t} = -L \frac{\delta F}{\delta P_i(r,t)} , (i = 1, 2, 3)$$
 (1)

where L represents the kinetic coefficient related to the domain wall mobility, t is time, r is the spatial position, F denotes the total free energy of the system. The total free energy of a ferroelectric membrane is given as²⁵,

$$F = \int_{V} (f_{\text{land}} + f_{\text{grad}} + f_{\text{electric}} + f_{\text{elastic}} + f_{\text{flexo}}) dV$$
 (2)

A polynomial function expanded to eighth order is adopted to describe the Landau free energy density $f_{\rm land}$, i.e.,

$$f_{\text{land}} = a_1 \sum_{i} P_i^2 + a_{11} \sum_{i} P_i^4 + a_{12} \sum_{i>j} P_i^2 P_j^2 + a_{111} \sum_{i} P_i^6 + a_{112} \sum_{i+j} P_i^4 P_j^2 + a_{123} \prod_{i} P_i^2 + a_{1111} \sum_{i} P_i^8 + a_{1112} \sum_{i+j} P_i^6 P_j^2 + a_{1122} \sum_{i>j} P_i^4 P_j^4 + a_{1123} \sum_{i+j+k,j>k} P_i^4 P_j^2 P_k^2$$
(3)

where a_i , a_{ij} , a_{ijk} , and a_{ijkl} are the Landau-Devonshire coefficients. The gradient energy density f_{grad} is expressed as,

$$f_{\text{grad}} = \frac{1}{2} G_{ijkl} P_{i,j} P_{k,l} \tag{4}$$

where G_{ijkl} is the gradient energy coefficients, $P_{i,j} = dP_i/dx_j$. The electrostatic energy density f_{electric} of the system is given by,

$$f_{\text{electric}} = -P_i E_i - \frac{1}{2} \varepsilon_0 k_{ij} E_i E_j \tag{5}$$

where E_i is the electric field component, ε_0 denotes the vacuum permittivity, k_{ij} is the dielectric constant. The flexoelectric energy density $f_{\rm flexo}$ can be written as,

$$f_{\text{flexo}} = -\frac{1}{2} f_{ijkl} (\varepsilon_{ij,k} P_k - \varepsilon_{ij} P_{k,l}) \tag{6}$$

where f_{ijkl} is the flexoelectric coefficient tensor. The elastic energy density $f_{\rm elastic}$ can be written as,

$$f_{\text{elastic}} = \frac{1}{2} C_{ijkl} e_{ij} e_{kl} = \frac{1}{2} C_{ijkl} (\varepsilon_{ij} - \varepsilon_{ij}^0) (\varepsilon_{kl} - \varepsilon_{kl}^0)$$
 (7)

where C_{ijkl} is the elastic stiffness coefficient tensor, e_{ij} is the elastic strain, ε_{ij} and ε_{ij}^0 are the total strain (i.e., the external applied strain) and the eigenstrain strain, respectively. The eigenstrain includes two parts: one from the electrostriction $\varepsilon_{ij}^{0'} = Q_{ijkl}P_kP_l$, where Q_{ijkl} is the electrostrictive coefficient, and the other from the flexoelectric effect $\varepsilon_{ij}^{0''} = f_{ijkl}P_{k,l}$.

The electric field (E_i) in Eq. (5) is solved by the electrostatic equilibrium equation without considering the charge carriers such as electrons, holes, and charged defects in the current study, i.e.,

$$D_{i,j} = \varepsilon_0 k_{ij} E_{i,j} + P_{i,j} = 0 \tag{8}$$

where D_i is the electric displacement. The open-circuit boundary condition is applied to the Ba_{1-x}Sr_xTiO₃ membrane for solving the electrostatic equilibrium equation.

The local strain and stress in Eq. (7) are obtained by solving the mechanical equilibrium equation, which is expressed as,

$$\sigma_{ij,j} = 0 \tag{9}$$

where σ_{ij} is the stress component, and $\sigma_{ij,j} = \frac{d\sigma_{ij}}{dx_i}$.

In this study, the TDGL equation, mechanical, and electrostatics equilibrium equations are solved by using the finite element method via COMSOL Multiphysics. The film thickness is assumed to be 20 nm. The total simulation size of the freestanding Ba_{1-x}Sr_xTiO₃ membranes is chosen to be $100 \Delta x \times 1 \Delta y \times 20 \Delta z$, with $\Delta x = \Delta y = \Delta z$ set to be 1.0 nm. Along the y direction, the periodic boundary condition for polarization P is applied when solving the TDGL and electrostatic equilibrium equations. The simulation coefficients and parameters are listed in Table S1 in Supplementary Information. To simulate the mechanical bending, the left and right edges of the membrane are set as the loading ends and tilted by θ degree along the y axis, which allows us to bend the membrane into different curvatures, as schematically shown in Fig. 1a and b. The top and bottom surfaces of the free-standing membrane are assumed to be stress free. The details of the boundary conditions for bended membranes are described in the Supplementary information. After bending, tensile strained and compressive strained regions are created in the top and bottom layers, as shown in Fig. S1 in the Supplementary information.

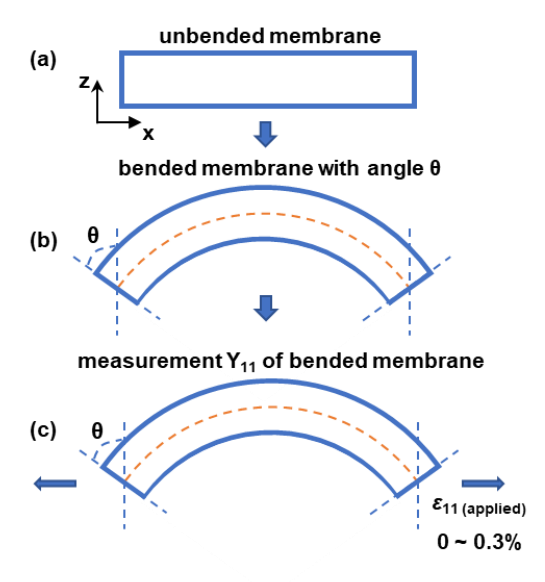


Fig. 1 Schematic of freestanding $Ba_{1-x}Sr_xTiO_3$ membrane under mechanical bending. (a) unbended membrane, (b) a bended membrane by tilting θ along y direction. θ is the bending angle. (c) the measurement of Young's modulus of bended $Ba_{1-x}Sr_xTiO_3$ by applying an in-plane tensile strain up to $\varepsilon_{11(applied)} = 0.3\%$.

To investigate the mechanically tunable Young's modulus of membranes via bending, we first relax the ferroelectric domain structure of Ba_{1-x}Sr_xTiO₃ membranes under different bending angles to reach equilibrium. Then, an external uniaxial tensile strain $\varepsilon_{ij(\text{applied})}$ is applied along the x direction of the bended membrane, and gradually increases from 0% to 0.3% to mimic the uniaxial tensile test to obtain the strain-stress curve, as shown in Fig. 1c. The actual Young's modulus along x direction (Y_{ij}) can be evaluated from the change of stress (σ_{ij}) in response to the externally applied strain ($\varepsilon_{ij(\text{applied})}$), which is described as Eq. (10). The details of the derivations of the Y_{11} are described in the Supplementary information.

$$Y_{ij} = \frac{d\sigma_{ij}}{d\varepsilon_{ij(\text{applied})}} = \frac{d(c_{ijkl}\varepsilon_{kl} - q_{ijkl}P_kP_l + \frac{1}{2}f_{ijkl}P_{k,l})}{d\varepsilon_{ij(\text{applied})}}$$
(10)

Based on the Eq. (10), it is seen that for the ferroelectric $Ba_{1-x}Sr_xTiO_3$ thin film, the polarization structures under different bending conditions highly affect the actual Y_{ij} . In this work, we mainly focus on the in-plane Young's modulus along x direction (Y_{11}).

Fig. 2a-c show the strain-stress curves of $Ba_{1-x}Sr_xTiO_3$ membranes at three typical compositions (i.e., ferroelectric $BaTiO_3$, weak-ferroelectric $Ba_{0.8}Sr_{0.2}TiO_3$, and paraelectric $Ba_{0.6}Sr_{0.4}TiO_3$) under different mechanical bending angles, respectively. For unbended $Ba_{1-x}Sr_xTiO_3$ membranes, nonlinear strain-stress curves are seen at all three compositions (black curves in Fig. 2a-c), resulting in variable Young's moduli (Y_{11}). This is probably caused by the ferroelectric domain evolutions under applied strain. Compared with the unbended membranes, the stress increases linearly with the increasing strain, resulting in a uniform elastic modulus (Y_{11}) for bended membranes at all three compositions (red, blue and green curves in Fig. 2a-c). In addition, as the bending angles increases from 5° to 30°, the calculated Y_{11} gradually increases. Our simulation results indicate that the actual Young's modulus can be precisely controlled by mechanical bending in both ferroelectric and paraelectric $Ba_{1-x}Sr_xTiO_3$ membranes.

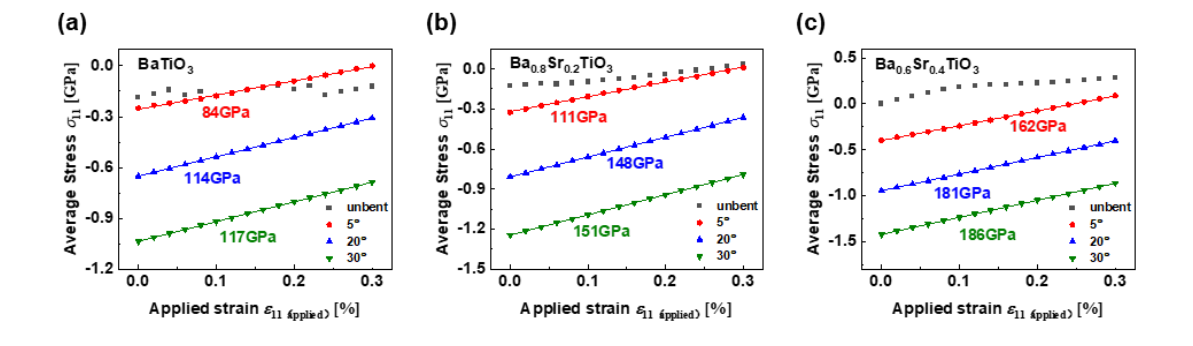


Fig. 2 The strain-stress curve and corresponding Young's modulus of Ba_{1-x}Sr_xTiO₃ membranes under increasing bending angles with three typical compositions as (a) BaTiO₃, (b) Ba_{0.8}Sr_{0.2}TiO₃, (c) Ba_{0.6}Sr_{0.4}TiO₃.

To quantitatively analyze the percentage change of Young's modulus by the mechanical bending, we define the tunability of Young's modulus as,

Tunability (%) =
$$\frac{Y_{11}^0 - Y_{11}^0}{Y_{11}^0}$$
 (11?)

where Y_{11}^{θ} is the Young's modulus under mechanical bending at θ . Y_{11}^{θ} is the Young's modulus at the reference state. By convention, the reference state is selected to be the unbended state. However, since a large variation in Y_{11} is seen in unbended Ba_{1-x}Sr_xTiO₃ membranes, we select the Young's modulus at bending angle $\theta = 5^{\circ}$ as the reference state. The tunability of Y_{11} as a function of bending angles at different compositions (x in Ba_{1-x}Sr_xTiO₃) is summarized in Fig. 3. It is observed that at all compositions, the tunability of Ba_{1-x}Sr_xTiO₃ membranes increases gradually with increasing θ , and eventually reaches a saturation value. The maximum tunability of ~ 40% is seen in pure BaTiO₃ when subjected to 30° bending. In addition, at given bending angle, the tunability decreases with increasing Sr²⁺ content (x). A significant tunability drop is seen between x = 0.3 (green curve) and x = 0.4 (purple curve), which is attributed to the ferroelectric-paraelectric transition near Sr²⁺ composition of 0.3.

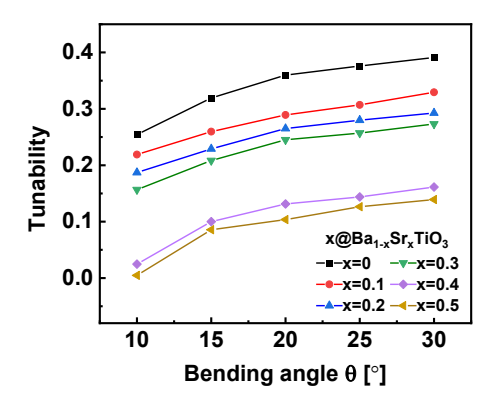


Fig. 3 The effect of bending angle on the Young's modulus tunability in Ba_{1-x}Sr_xTiO₃ membranes

A large deformation caused by the mechanical bending can induce ferroelectric domain switching in membranes, which further influences their elastic properties²³. To understand the underlying mechanism of Young's modulus tunability induced by mechanical bending in Ba_{1-x}Sr_xTiO₃ membranes, we analyze the ferroelectric domain structure under different bending conditions as illustrated in Fig. 4a-c. The left and right panels in Fig. 4a-c are the equilibrium domain structures before and after applying the tensile strain. For unbended ferroelectric BaTiO₃ membrane, the domain structure is mainly composed of a mixture of $a(\pm 1,0,0)$ and $c(0,0,\pm 1)$ domains which form a flux-closure pattern (① in Fig. 4a). When an external tensile strain of 0.3 % is applied on the unbended film, almost all the c domains transform into a domains (② in Fig. 4a). The $c \rightarrow a$ domain switching leads to an evident change of the elastic strain distribution (e_{ij}) at fixed applied strain (ε_{ij}) based on Eq. 7, due to a large variation in the eigenstrain induced by the different polarization configuration (Figs. S3 and S4). This results in a nonlinear strain-stress curve (black curve in Fig. 2a) and a large variation in the Young's modulus at unbended state.

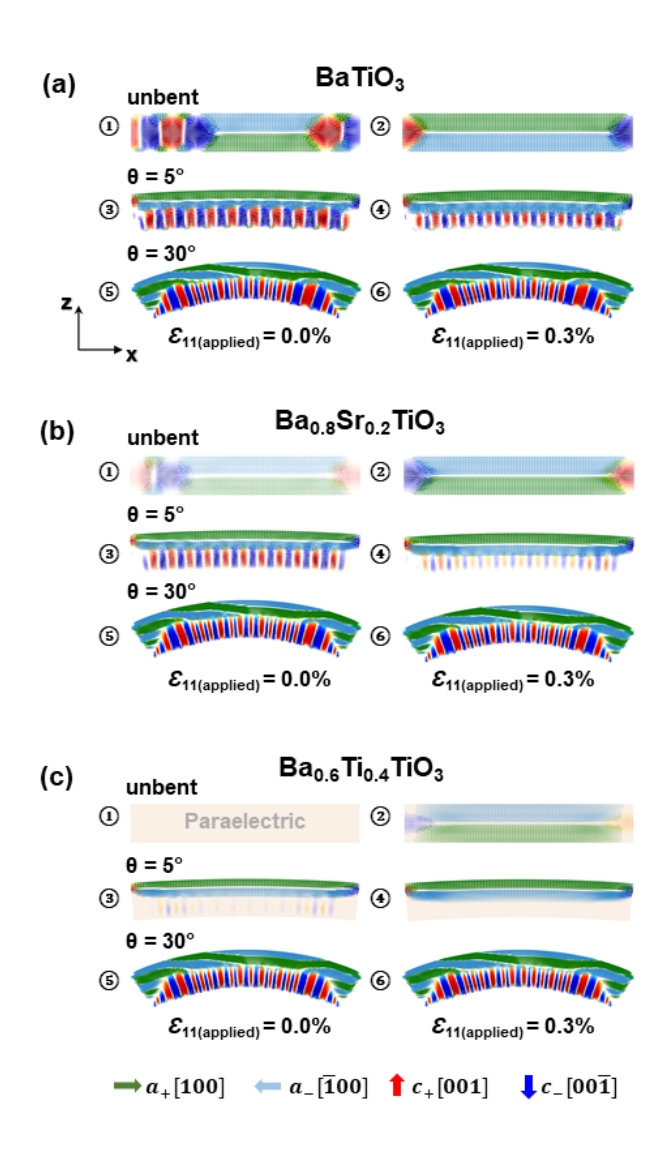


Fig.4 Ferroelectric domain structures of the freestanding $Ba_{1-x}Sr_xTiO_3$ membranes upon different bending angles with three typical compositions corresponding to (a) $BaTiO_3$, (b) $Ba_{0.8}Sr_{0.2}TiO_3$, (c) $Ba_{0.6}Sr_{0.4}TiO_3$. The membranes at the state of without applying the external tensile strain $\varepsilon_{11(applied)} = 0\%$ is at the left panel and their corresponding domain structures under an additional tensile strain $\varepsilon_{11(applied)} = 0.3\%$ is at right panel. The arrows represent the orientation of the local polarization.

For pure BaTiO₃ membrane at 5° bending state, a maximum tensile/compressive strain of $\pm 1.9\%$ are induced at the top/bottom surfaces. In the tensile strain region, the lattice has been stretched along x direction and the domain structure switches to a domain with 180° domain walls, while c domains exist in the compressive strain region caused by

the compressed lattice. Correspondingly, a vortex-like patterns have been generated and the vortex cores are located at the junction of a/c domains ((3) in Fig. 4a). When an external tensile strain ($\varepsilon_{11(applied)} = 0.3\%$) is applied on the bended film, the magnitude of P_1 in the tensile strain region (z = 19 nm) slightly increases, and P_3 in the compressed region (z = 2nm) decreases as shown in Fig. S2a and b, which corresponds a slight c to a domain switching under the external tensile strain for a bended membrane. Although there is small change in the magnitude of polarization in c and a domains for a bended membrane under 0.3% tensile strain, it still shows the vortex structure pattern without major changes ((4) in Fig. 4a). As a result, a linear strain-stress relation and a uniform Young's modulus can be obtained (red curve in Fig. 2a), compared with the unbended membrane (black curve in Fig. 2a). As the bending angle further increases to 30°, the maximum surface tensile/compressive strain reaches $\pm 10\%$. Large bending deformation contributes to the magnitudes of polarization (P_1 and P_3) and the number of vortex-like structure increase ((5) in Fig. 4a). After a 0.3% external strain is applied, the domain structure ((6) in Fig. 4a) and the magnitude of polarization component (Fig. S2a and b) remain almost unchanged, which means that there is almost no c to a domain switching under 0.3% tensile strain in the bended membrane subjected to a large bending angle of 30°.

We also investigate the effect of Sr^{2+} content (x) on the domain evolution and the corresponding Young's modulus tunability. When x increases, $Ba_{1-x}Sr_xTiO_3$ experiences a ferroelectric-paraelectric transition, as shown in Fig. 4a-c. For unbended $Ba_{0.8}Sr_{0.2}TiO_3$ membrane (1) in Fig. 4b), it shows a similar behavior to $BaTiO_3$ membrane that an evident domain switching from c to a under an external tensile strain, which results in a nonlinear

strain-stress relation and a variation in Young's modulus (black curve in Fig. 3b). For the unbended paraelectric Ba_{0.6}Sr_{0.4}TiO₃ film, the ferroelectric phases (a domain) are generated under the external tensile strain (2 in Fig. 4c). This paraelectric-ferroelectric transformation leads to a transition in Young's modulus (black curve in Fig. 2c). However, for both Ba_{0.8}Sr_{0.2}TiO₃ and Ba_{0.6}Sr_{0.4}TiO₃ freestanding membranes, the enhancing polarization with a vortex structure is induced by mechanical bending (left panel in Fig. 4b and c). Similar to BaTiO₃ membrane, a slight change in the magnitude of polarization components P_1 and P_3 (Fig. S2 c-f) and a nearly unchanged vortex structure patterns after the application of additional external tensile strain (right panel in Fig. 4b and c) implies that c to a domain switching is inhibited for bended membranes. Thus, an increasing Young's modulus tunability with bending angle is illustrated for all Ba_{1-x}Sr_xTiO₃ membranes (Fig. 3).

Based on our simulations, the c to a domain switching under an external tensile strain is inhibited for the bended Ba_{1-x}Sr_xTiO₃ membranes compared with the unbended ones. To further understand this phenomenon, we investigate the gradient energy density (f_{grad}) of a freestanding BaTiO₃ membrane as a function of bending angle (θ) , as shown in Fig. 5a. From Fig. 5a, f_{grad} increases almost linearly with increasing θ . This can be explained by the decrease of average domain sizes and the increase of numbers of 180° domain walls (separating $c_+(0,0,1)$ and $c_-(0,0,\overline{1})$) and the vortex-like domain walls as bending angle θ increases. The increasing gradient energy density further inhibits the c to a domain switching under the external tensile strain. Thus, the limited domain switching in highly bended membrane results in almost identical eigenstrain (e_{ij}^0) distributions before

and after a tensile strain ($\varepsilon_{11(applied)}$) is applied (Fig. S3 c-f), and consequently a larger Young's modulus based on the Eq. (13). That explains why the Young's modulus increases with increasing bending angle in Ba_{1-x}Sr_xTiO₃ membranes (Fig. 2).

In addition, Fig. 5b shows that the domain wall energy of bended $Ba_{1-x}Sr_xTiO_3$ membranes decreases gradually with increasing Sr^{2+} content at given bending angle state $(\theta = 15^{\circ})$. The reduction in the gradient energy implies that domain switching becomes relatively easier under external tensile strain in bended $Ba_{1-x}Sr_xTiO_3$ membrane with higher Sr^{2+} content, leading to a reduction in the corresponding Young's modulus. That explains why the tunability of Young's modulus of $Ba_{1-x}Sr_xTiO_3$ system decreases with increasing Sr^{2+} content (Fig. 3).

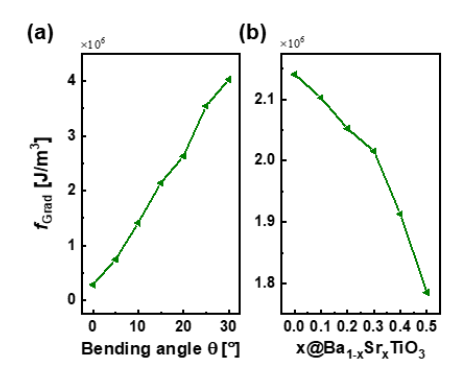


Fig. 5 The gradient energy density (f_{grad}) of the freestanding Ba_{1-x}Sr_xTiO₃ membranes as the function of (a) bending angle θ (with the composition of x = 0, BaTiO₃) and (b) Sr²⁺ content (at a given bending angle state $\theta = 15^{\circ}$).

In summary, a phase-field simulation is developed to reveal the Young's modulus tunability under mechanical bending in $Ba_{1-x}Sr_xTiO_3$ membranes. The results demonstrate that unlike the unbended freestanding membranes with a large variation in the Young's modulus, the bended $Ba_{1-x}Sr_xTiO_3$ membranes show a uniform Young's modulus. With increasing bending angle, the tunability of Young's modulus is enhanced. This can be

attributed to the vortex-like domain structures induced by the bending deformation. For the bended Ba_{1-x}Sr_xTiO₃ membranes, the magnitude of polarization and the number of vortex-like structures increases with the increasing bending angle, which leads to the increase of domain wall energy. The larger domain wall energy further inhibits the subsequent domain switching under external tensile stress and reduces the variation in the polarization induced eigenstrain. This eventually leads to a large Young's modulus. Moreover, we also investigate the effect of Sr²⁺ content on the tunability of Young's modulus. At the same bending state, the magnitude of polarization in the vortex domain structures are gradually suppressed as Sr²⁺ content increases, resulting in a reduction of gradient energy density. Consequently, the Young's modulus tunability decreases with increasing Sr²⁺ content. This work provides a fundamental understanding of the mechanical tunability in Ba_{1-x}Sr_xTiO₃ membranes, as well as an opportunity for achieving precisely controllable Young's modulus by mechanical bending in freestanding membranes, which is important for designing the flexible electronic devices.

See the supplementary materials for the details of boundary conditions, polarization component distributions, eigenstrain and elastic strain distributions, and simulation parameters.

The authors acknowledge the support from the National Science Foundation (NSF 2132105), and the Texas Advanced Computing Center (TACC) at The University of Texas at Austin for providing HPC resources. We would also like to thank Changqing Guo (Beijing Institute of Technology) and Dr. Joseph H Ngai (University of Texas at Arlington) for the useful discussions.

The data that support the findings of this study are available from the corresponding author upon reasonable request.

- ¹ H. Zhang, T. Wei, Q. Zhang, W. Ma, P. Fan, D. Salamon, S.-T. Zhang, B. Nan, H. Tan, and Z.-G. Ye, J. Mater. Chem. C **8**, 16648 (2020).
- ² M.-J. Zhou, T. Yang, J.-J. Wang, Z. Ren, L.-Q. Chen, and C.-W. Nan, Acta Mater. **187**, 146 (2020).
- ³ S. Zhang, F. Li, X. Jiang, J. Kim, J. Luo, and X. Geng, Prog. Mater. Sci. 68, 1 (2015).
- ⁴ C. Xu, F. Cai, S. Xie, F. Li, R. Sun, X. Fu, R. Xiong, Y. Zhang, H. Zheng, and J. Li, Phys. Rev. Appl. **4**, 034009 (2015).
- ⁵ JAMES F Scott, **246**, 7 (n.d.).
- W. Xiong, L. Liu, J. Liu, W. Chen, and Y. Zheng, Appl. Phys. Lett. 118, 242902 (2021).
- ⁷ H. Fu and R.E. Cohen, Nature **403**, 281 (2000).
- ⁸ J.X. Zhang, B. Xiang, Q. He, J. Seidel, R.J. Zeches, P. Yu, S.Y. Yang, C.H. Wang, Y.-H. Chu, L.W. Martin, A.M. Minor, and R. Ramesh, Nat. Nanotechnol. 6, 98 (2011).
- ⁹ T. Li, A. Lipatov, H. Lu, H. Lee, J.-W. Lee, E. Torun, L. Wirtz, C.-B. Eom, J. Íñiguez, A. Sinitskii, and A. Gruverman, Nat. Commun. **9**, 3344 (2018).
- ¹⁰ L. Keeney, T. Maity, M. Schmidt, A. Amann, N. Deepak, N. Petkov, S. Roy, M.E. Pemble, and R.W. Whatmore, J. Am. Ceram. Soc. **96**, 2339 (2013).
- ¹¹ D. Pesquera, E. Parsonnet, A. Qualls, R. Xu, A.J. Gubser, J. Kim, Y. Jiang, G. Velarde, Y. Huang, H.Y. Hwang, R. Ramesh, and L.W. Martin, Adv. Mater. 32, 2003780 (2020).
- ¹² R. Xu, J. Huang, E.S. Barnard, S.S. Hong, P. Singh, E.K. Wong, T. Jansen, V. Harbola, J. Xiao, B.Y. Wang, S. Crossley, D. Lu, S. Liu, and H.Y. Hwang, Nat. Commun. 11, 3141 (2020).
- ¹³ B. Wang, H. Lu, C.W. Bark, C.-B. Eom, A. Gruverman, and L.-Q. Chen, Acta Mater. 193, 151 (2020).
- ¹⁴ R.J. Zeches, M.D. Rossell, J.X. Zhang, A.J. Hatt, Q. He, C.-H. Yang, A. Kumar, C.H. Wang, A. Melville, C. Adamo, G. Sheng, Y.-H. Chu, J.F. Ihlefeld, R. Erni, C. Ederer, V. Gopalan, L.Q. Chen, D.G. Schlom, N.A. Spaldin, L.W. Martin, and R. Ramesh, Science 326, 977 (2009).
- ¹⁵ W. Xiong, J. Liu, L. Ma, W. Chen, and Y. Zheng, J. Appl. Phys. **128**, 014102 (2020).
- ¹⁶ H. Ma, G. Yuan, T. Wu, Y. Wang, and J.-M. Liu, ACS Appl. Mater. Interfaces 10, 40911 (2018).
- ¹⁷ Y.L. Li, S.Y. Hu, Z.K. Liu, and L.Q. Chen, Acta Mater. **50**, 395 (2002).
- ¹⁸ G. Dong, S. Li, M. Yao, Z. Zhou, Y.-Q. Zhang, X. Han, Z. Luo, J. Yao, B. Peng, Z. Hu, H. Huang, T. Jia, J. Li, W. Ren, Z.-G. Ye, X. Ding, J. Sun, C.-W. Nan, L.-Q. Chen, J. Li, and M. Liu, Science 366, 475 (2019).
- ¹⁹ C. Jin, Y. Zhu, X. Li, F. An, W. Han, Q. Liu, S. Hu, Y. Ji, Z. Xu, S. Hu, M. Ye, G. Zhong, M. Gu, and L. Chen, Adv. Sci. 8, 2102178 (2021).
- ²⁰ R.-C. Peng, X. Cheng, B. Peng, Z. Zhou, L.-Q. Chen, and M. Liu, Acta Mater. 208, 116689 (2021).
- ²¹ D.L. Ko, M.F. Tsai, J.W. Chen, P.W. Shao, Y.Z. Tan, J.J. Wang, S.Z. Ho, Y.H. Lai, Y.L. Chueh, Y.C. Chen, D.P. Tsai, L.-Q. Chen, and Y.H. Chu, Sci. Adv. 6, eaaz3180 (2020).
- ²² C. Guo, G. Dong, Z. Zhou, M. Liu, H. Huang, J. Hong, and X. Wang, Appl. Phys. Lett. 116, 152903 (2020).

²³ G. Dong, S. Li, T. Li, H. Wu, T. Nan, X. Wang, H. Liu, Y. Cheng, Y. Zhou, W. Qu, Y. Zhao, B. Peng, Z. Wang, Z. Hu, Z. Luo, W. Ren, S.J. Pennycook, J. Li, J. Sun, Z. Ye, Z. Jiang, Z. Zhou, X. Ding, T. Min, and M. Liu, Adv. Mater. **32**, 2004477 (2020).

Z. Jiang, Z. Zhou, X. Ding, T. Min, and M. Liu, Adv. Mater. **32**, 2004477 (2020). ²⁴ Y.H. Huang, J.J. Wang, T.N. Yang, Y.J. Wu, X.M. Chen, and L.Q. Chen, Appl. Phys. Lett. **112**, 102901 (2018).

²⁵ L.-Q. Chen, J. Am. Ceram. Soc. **91**, 1835 (2008).